Clim Dyn
DOI 10.1007/s00382-010-0803-5

Natural forcing of climate during the last millennium: fingerprint of solar variability

Low frequency solar forcing and NAO

D. Swingedouw · L. Terray · C. Cassou · A. Voldoire · D. Salas-Mélia · J. Servonnat

Received: 14 August 2009 / Accepted: 22 March 2010

Abstract The variability of the climate during the last millennium is partly forced by changes in total solar irradiance (TSI). Nevertheless, the amplitude of these TSI changes is very small so that recent reconstruction data suggest that low frequency variations in the North Atlantic Oscillation (NAO) and in the thermohaline circulation may have amplified, in the North Atlantic sector and mostly in winter, the radiative changes due to TSI variations. In this study we use a state-of-the-art climate model to simulate the last millennium. We find that modelled variations of surface temperature in the Northern Hemisphere are coherent with existing reconstructions. Moreover, in the model, the low frequency variability of this mean hemispheric temperature is found to be correlated at 0.74 with the solar forcing for the period 1001–1860. Then, we focus on the regional climatic fingerprint of solar forcing in winter and find a significant relationship between the low frequency TSI forcing and the NAO with a time lag of more than 40 years for the response of the NAO. Such a lag is larger than the around 20-year lag suggested in other studies. We argue that this lag is due, in the model, to a northward shift of the tropical atmospheric convection in the Pacific Ocean, which is maximum more than four decades after the solar forcing increase. This shift then forces a positive NAO through an atmospheric wave connection related to the jet-stream wave guide. The shift of the tropical convection is due to the persistence of anomalous warm SST forcing the anomalous precipitation, associated with the advection of warm SST by the North Pacific subtropical gyre in a few decades. Finally, we analyse the response of the Atlantic meridional overturning circulation to solar forcing and find that the former is weakened when the latter increases. Changes in wind stress, notably due to the NAO, modify the barotropic streamfunction in the Atlantic 50 years after solar variations. This implies a wind-driven modification of the oceanic circulation in the Atlantic sector in response to changes in solar forcing, in addition to the variations of the thermohaline circulation.

Keywords Last millennium · Natural climate variability · Solar forcing · North Atlantic Oscillation · Thermohaline circulation

D. Swingedouw · L. Terray · C. Cassou
CERFACS, 42 Av. G. Coriolis, 31057 Toulouse, France

A. Voldoire · D. Salas-Mélia
CNRM, 42 Av. G. Coriolis, 31057 Toulouse, France

J. Servonnat
LSCE/IPSL, CEA Saclay, Orme des Merisiers,
91191 Gif-sur-Yvette, France

Present Address:
D. Swingedouw (✉)
LSCE/IPSL, CEA Saclay, Orme des Merisiers,
91191 Gif-sur-Yvette, France
e-mail: Didier.Swingedouw@lsce.ipsl.fr

1 Introduction

The climate system fluctuates over a very large range of frequency. For instance, global surface temperature varies on time scales going from days to millions of years (Huybers and Curry 2006). These fluctuations can be internal to the climate system, which means that they are inherent to the different components of the system and to their interactions. They can also be forced by natural forcing like the variations in total solar irradiance (TSI) or volcanic eruptions. These internal and naturally forced variabilities are usually called "natural variability", in opposition to the variability forced by anthropogenic greenhouse gases emissions.

Published online: 09 April 2010

The multi-decadal variability of climate is of particular interest for society because this time scale is similar to that of a human life and can strongly affect the climate of a given region for a long period (Paillard 2008). Moreover, the projected global warming induced by anthropogenic greenhouse gases emissions has raised the question of how much of the recent observed warming is related to anthropogenic perturbation from that due to natural variability. The last IPCC report (Hegerl et al. 2007) shows that it is very likely that the warming observed over the last decades is due to anthropogenic perturbation. Nonetheless, it has also been shown that natural climate variability can strongly modulate the future warming trend (Keenlyside et al. 2008) especially over the next two or three decades.

Understanding the multi-decadal natural variability of the climate system is a difficult challenge because (1) the instrumental observations of the climate system only go back to 1850 or so and (2) the numerical simulations designed to investigate the multi-decadal variability of the climate necessitate very long integrations of climate models, which are very costly in terms of computer resources. To circumvent (1), climate reconstructions for the last few millennia with a very high temporal resolution have been realised by using different paleo-climate proxies like tree rings, ice cores, documentary sources, boreholes (Bradley and Jones 1993; Mann et al. 1998; Jones et al. 2001; Moberg et al. 2005; Mann et al. 2008 among many others). All these reconstructions have tried to capture the surface temperature evolution of the Northern Hemisphere. They have put forward the existence of a Medieval Warm Epoch (Lamb 1965) at the beginning of the last millennium and of a Little Ice Age (Eddy 1976) from around 1400 to 1800.

One of the most classical hypotheses to explain these climate evolutions is related to the TSI variability, which can be reconstructed using sunspot numbers and cosmogenic isotopes production like ^{10}Be or ^{14}C. Bard et al. (2000), by using these cosmogenic isotopes records, has proposed a reconstruction of the TSI for the last millennium. Although the scaling used for this reconstruction is under debate (Lean et al. 2002; Foukal et al. 2004), other reconstructions (Muscheler et al. 2007) confirm the time evolution of solar variability with clear minima of solar activity like the Maunder ($\sim$1700) and Dalton ($\sim$1810) Minima.

The impact of solar forcing on climate is first due to the radiative forcing implied by the variations in TSI. This radiative forcing is not homogeneous in space and evolves with the cosine of the latitude and is thus maximum at the equator. Moreover, it has been proposed that solar variability may influence the occurrence of natural modes of variability and in particular the North Atlantic Oscillation (NAO). The NAO can be defined as the first mode of sea level pressure (SLP) variability over the Atlantic sector in winter (Hurrell 1995). It has a large influence upon the climate of Europe and is characterized in its positive phase by a warming over northern Europe associated with increased westerlies and a cooling over the Mediterranean area. Shindell et al. (2001, 2003) compared simulations from an Atmosphere General Circulation Model (AGCM) coupled to a slab ocean and spatial reconstructions for the period 1680–1780, including the Maunder Minimum. They found a clear signature of TSI changes on surface temperature resembling the one linked to the NAO negative phase, lagging the changes in solar variability by 20 years. They explained this effect by the decrease in the meridional gradient of lower stratospheric temperature, affecting the jet-stream, which leads to a negative NAO through atmospheric wave dynamics. They explained the 20-year lag as the time scale necessary for the tropical ocean to adjust in response to the solar forcing and transmit the surface thermal signal to the lower stratosphere. Such a relation between solar forcing and NAO has been confirmed in paleo-data by Waple et al. (2002). The latter also showed that the link between solar forcing and the NAO is even longer for a lag of as much as 30 years (see their Fig. 7). This relationship between solar forcing and the NAO has also been found in coupled ocean–atmosphere GCM (OAGCM) simulations by Zorita et al. (2004) and Stendel et al. (2006).

Most of the previous studies do not analyse the climatic response to solar forcing over the Pacific Ocean. Shindell et al. (2001, 2003) did not use a dynamical ocean model, so that the coupled ocean–atmosphere feedbacks are poorly resolved in their model. Zorita et al. (2004) focused on the North Atlantic and noticed that solar forcing reduces the Atlantic meridional overturning circulation (AMOC) as in projections of future global warming (Schneider et al. 2007), while Stendel et al. (2006) found a very small impact of solar forcing on the North Atlantic. Both studies do not focus on the Pacific response, which can nevertheless strongly impact on the NAO (Cassou and Terray 2001). More recently, Meehl et al. (2008) analysed the response of the Pacific Ocean to the 11-year solar cycle (Schwabe cycle) during the last century. They found, using recent observations and OAGCM ensemble simulations, a coupled air–sea mechanism in boreal winter in response to the solar maxima, which can be compared to La Nina events. The proposed mechanism works as follows: the equatorial and tropical regions receive most of the solar irradiance so that TSI variations are maximum at these locations in terms of short wave at the top of the atmosphere. The surface of these regions can therefore accumulate energy during solar maxima. However, Meehl et al. (2008) showed that in the Pacific Ocean, the sea surface temperature (SST) does not increase very much in response

to TSI variations because most of the energy accumulated in the surface ocean is rapidly released to the atmosphere through latent heat flux (which cools the SST). This release is associated with an increased zonal moisture transport towards the western warm pool, an increase in atmospheric convection there, and a slight northward shift of the Inter-Tropical Convergence Zone (ITCZ). The Walker cell is therefore enhanced, which increases the subsidence in the eastern Pacific, leading to a decrease in cloud cover and an increase in downward shortwave radiation, which feeds back positively on the whole mechanism. This feedback is fast (a few months) so that it operates in the Schwabe cycle time-frame.

In the present study, we aim at evaluating the impact of low frequency (larger than the Schwabe cycle) TSI variations on climate. The main focus is put on the winter boreal season in order to understand the link between solar variability and climate in the North Atlantic region. In particular, we will show, using an OAGCM, that TSI variations can influence the low frequency of the NAO with a lag of around 40 years, through a slow adjustment of the Pacific Ocean to solar forcing. The paper is organised as follows: In Sect. 2, we describe the experimental design of the study. In Sect. 3, we evaluate the general response of climate to solar variability in our OAGCM. In Sect. 4, we focus on the boreal winter response of the NAO and Pacific Ocean. In Sect. 5, we evaluate the impact of solar forcing on the North Atlantic. Discussions and conclusions are given in Sect. 6.

2 Experimental design

2.1 Model description

The model used in this study is the CNRM-CM3.3 OAGCM. It is based on the coupled core formed by ARPEGE-Climat version 4.6 AGCM (Déqué et al. 1999; Gibelin and Déqué 2003) and OPA 8.1 OGCM (Madec et al. 1998). CNRM-CM3.3 also includes a sea ice model, GELATO2 (Salas-Mélia 2002), and the total runoff integrated pathways (TRIP) river routing scheme (Oki and Sud 1998; Chapelon et al. 2002). These components run on distinct grids and with different time steps and are coupled synchronously, exchanging information every 24 h through the OASIS coupling software (Valcke et al. 2004). The different components are briefly described in the following sections. Full details about CNRM-CM3.3 are given by Salas-Mélia et al. (2005).

2.1.1 The ARPEGE-Climat, ISBA and TRIP models

The representation of most model variables in ARPEGE-Climat is spectral. In the framework of this study, ARPEGE-Climat was run on an horizontal grid corresponding to a linear T63 truncation. All the physics and non-linear terms are treated on an associated Gaussian reduced grid (longitude–latitude grid of about 2.8° in horizontal resolution). The model has 31 levels on the vertical. In this version of ARPEGE, the direct effects of aerosols (sea salt, desert dust, black carbon and sulfates) are taken into account, as well as the indirect effects from sulfate aerosols. The semi-Lagrangian advection scheme allows for a 30-min time step. The ISBA soil-vegetation-atmosphere transfer model, described by Mahfouf et al. (1995) is included in ARPEGE-Climat. It contains a detailed snow cover formulation (Douville et al. 1995). Soil and vegetation properties are derived from the global high resolution ECOCLIMAP dataset (Masson et al. 2003) and are prescribed. ARPEGE-Climat uses ocean temperature, sea ice extent and albedo boundary conditions computed by the OPAGELATO system and interpolated by OASIS, and provides surface fluxes to the ocean-sea ice model. The total runoff is computed by ISBA and interpolated on a $1° \times 1°$ horizontal grid by means of OASIS. It is then converted into river discharge and transported to the ocean using TRIP. The water outflow produced at every river mouth is dumped in the closest ocean grid cells. As this amount of water can be huge for the biggest rivers, it is shared between several ocean grid cells (up to 10 for the Amazon) to avoid spurious ocean surface negative salinities. The time step used in TRIP in the framework of CNRM-CM3 is 3 h.

2.1.2 The OPA and GELATO models

The version of OPA8 OGCM used in CNRM-CM3 has a horizontal grid of 182×152 points, which roughly corresponds to a resolution of 2° in longitude, while in latitude, the grid point spacing decreases from about 2° in polar regions to 0.5° near the equator. The model has 31 vertical levels, 10 of them within the upper 100 m, and uses a z-coordinate mesh. It runs with a time step of 96 min. OPA8.1 is used here as a rigid lid model, hence uses a virtual freshwater flux, the sum of non solar heat fluxes (latent, sensible and net longwave fluxes) and the momentum flux provided by ARPEGE-Climat. The vertical eddy diffusivity and viscosity of the model are computed by using a 1.5 TKE turbulent closure scheme (Blanke and Delecluse 1993), while in the horizontal, an isopycnal diffusion scheme is applied, with an eddy viscosity of 40, 000 m^2/s for momentum and an eddy diffusivity equal to 2, 000 m^2/s for tracers. Convective mixing is parametrized by the non-penetrative convective adjustment algorithm implemented by Madec et al. (1991). Mixed layer depth is detected by a density difference of 0.01 kg/m^3 with the ocean surface. The penetration of sunlight is

formulated by means of two extinction coefficients (Paulson and Simpson 1977). The GELATO2 sea-ice model (Salas-Mélia 2002) is directly embedded in the ocean component of CNRM-CM3 and uses the same grid. Its time step is 24 h. The elastic-viscous-plastic dynamics by Hunke and Dukowicz (1997) is included, and the advection of sea ice slabs is semi-Lagrangian, as described by Hunke and Lipscomb (2002). Due to convergence, sea ice can raft (ice thinner than 0.25 m) or ridge (ice thicker than 0.25 m). These processes are taken into account by a redistribution scheme derived from Thorndike et al. (1975). GELATO2 has four different ice thickness categories: 0–0.3, 0.3–0.8, 0.8–3 and over 3 m. Transitions or mergers between these categories may occur as ice thickness varies thermodynamically. Every slab of ice is evenly divided into four vertical layers and may be covered with one layer of snow, for which snow aging processes are considered. The heat diffusion equation is solved along the vertical (Salas-Mélia 2002) through the entire slab. The impact of icebergs around the Antarctic is represented as additional water and latent heat fluxes due to the melting of ice. These fluxes are assumed to be evenly spread south of 60°S. This flux is applied only during the summer austral season (October–March) as a constant flux of ice of 0.14 Sv (1 Sv = 10^6 m^3 s^{-1}) over this period, which is both consistent with the modelled accumulation of snow over Antarctica estimated from a control experiment and with current observational estimates of the annual volume of calved icebergs.

2.2 Numerical experiments

In the present study we have performed two 1,000-year simulations. The first one (CTRL) is a pre-industrial control experiment similar to the one described in Guemas and Salas-Mélia (2008a). In this simulation, the CO_2 concentration is equal to 280 ppm, and the TSI is set to 1,370 W/m^2. The second simulation (MILL) has been designed to take into account the external climate forcing using state-of-the-art reconstructions for the volcanic eruptions, the TSI variations, the greenhouse gases concentration and the anthropogenic sulfate aerosols changes for the period 1001–2000.

The TSI variations that we use are deduced from the Bard et al. (2000) reconstruction and are the same as the one used by Crowley (2000). The variations for the solar radiative forcing averaged globally are represented in Fig. 1a and allow to identify the so-called Oort (~1060), Wolf (~1320), Spörer (~ 1460), Maunder (~1700) and Dalton (~1810) Minima of solar activity. The TSI anomalies are centered on the period 1860–2000 whose mean is chosen to be equal to 1,370 W/m^2 as in the CTRL simulation. The amplitude of the solar forcing variations for the TSI reconstruction that we use represents a 0.24% decrease of the mean TSI between present day and the Maunder Minimum (Lean et al. 1995). This scaling is under debate since Lean et al. (2002) or Foukal et al. (2004) suggest that long-term irradiance changes could be notably less. Nevertheless, no clear consensus has yet emerged on the best scaling for the solar irradiance. The solar radiative forcing that we choose remains nonetheless quite small as compared to anthropogenic greenhouse gases as shown in Fig. 1 with a total range of radiative forcing variations smaller than 1 W/m^2 over the millennium compared to the 2.4 W/m^2 due to anthropogenic greenhouse gases emissions in one century and a half.

The volcanic forcing that we use is based on the Ammann et al. (2007) reconstruction for the stratospheric injection of sulfate volcanic aerosols. This reconstruction

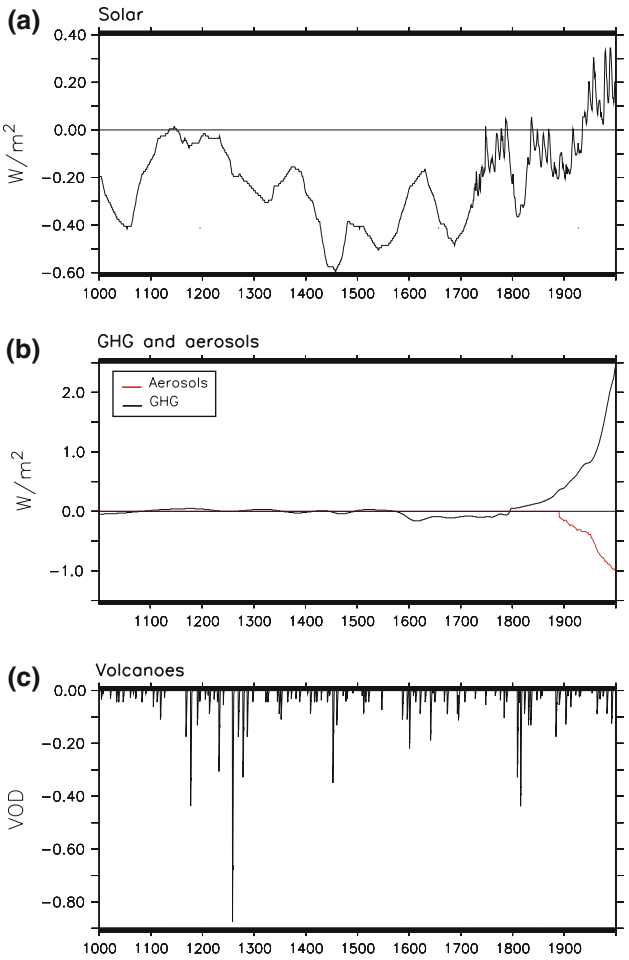

Fig. 1 Climatic forcing used in the simulation MILL. **a** Solar forcing expressed in terms of radiative forcing (in W/m^2) globally averaged on the sphere. The anomalous changes in TSI, which are centered on the period 1860–2000, can be obtained by multiplying by 4 and dividing by 0.7 (mean albedo of the Earth at the top of the atmosphere). **b** Greenhouse gases (GHG) and aerosols radiative forcing (in W/m^2). **c** Volcanic eruptions impact on the Visual Optical Depth (VOD) using data from Ammann et al. (2007)

uses data from ice cores records from Greenland and Antarctica. The volcanic aerosols in the stratosphere are transported latitudinally in the model following Grieser and Schönwiese (1999) parametrisation. We consider 48 latitude bands for this transport. The model incorporates prescribed changes in aerosol optical depth, and interactively computes the perturbed (longwave and shortwave) radiative budgets.

The greenhouse gases variations are also taken into account in the MILL simulation. Before 1860, we account for the CO_2 concentration variations, which explained the variations in radiative forcing appearing in Fig. 1b. After 1860, the simulation accounts for the increase in different greenhouse gases (CO_2, CH_4, N_2O, CFCs...) and also from 1890 for the anthropogenic aerosol emissions (Fig. 1b). The concentrations used are from the 20C3M simulation of the last IPCC (Forster et al. 2007). Moreover, the land-use changes as reconstructed by Ramankutty and Foley (1999) are also included from 1700. The land-use is fixed to its 1700 value for the period before 1700. Nevertheless, the associated changes in radiative forcing are almost negligible before around 1860. Orbital variations of the Earth in relation to the Sun, can be calculated accurately (Berger 1978). For the last millennium, their impact on climate can be neglected compared to the other forcings (Bertrand et al. 2002), so that we do not take them into account in the MILL simulation.

Both simulations start from the same initial conditions, which are derived from a spin-up simulation of 250 years starting from rest from Levitus (1982) for the ocean temperature and salinity, and a randomly chosen 1st January for the atmosphere. In the CTRL simulation the net heat flux budget at the surface equals 0.33 W/m^2 when averaged over 1,000 years. Consequently there is a slight drift for the SST in CTRL of 0.027 K/century and of 0.039 K/ century for the ocean deeper than 1,000 m.

In the present paper, we choose to focus on the low frequencies variability of climate related to TSI variability. Since the MILL experiment is forced with different external forcing, notably the volcanic forcing, it is not straightforward to identify the solar effect on climate. Nevertheless, impact of volcanic eruption occurs at high frequency: it is supposed to affect the climate for 2–3 years only (Ottera 2008). We will analyse its impact on climate in this simulation as compared to available reconstruction in a companion paper. To minimize the climatic signature of the volcanoes in the present study, we apply a low-pass Lanczos time-filter (Duchon 1979) to all the fields analysed next, with a cutoff values of 13 years at least. Moreover we detrend all the variables of MILL by using the linear trend extracted from CTRL. This has been done to eliminate the linear trend due to model biases. The approximation of linear trend has been tested by removing a quadratic trend but it does not modify the results presented hereafter so that we keep the linear trend hypothesis. Finally, the statistical significance of the correlations computed in this study are estimated by using a "random-phase" test that accounts for the serial correlation effect due to the low-pass filtering of the data (Ebisuzaki 1997).

3 Low frequency variability of surface temperature

3.1 Hemispheric variability

In Fig. 2 is shown the Northern Hemisphere annual mean surface temperature of the MILL simulation, smoothed with a 30 year cutoff filter. This low frequency variability lies in the interval of the reconstructions overlap of Jansen et al. (2007, Fig. 6.10 of chapter 6), representing ten Northern Hemisphere temperature reconstructions and their associated uncertainty ranges. This overlap gives a good view of the temperature range covered by the temperature reconstructions obtained from data. From this overlap we have drawn the curve corresponding to the most likely value of the temperature for each year. This curve helps to evaluate the most likely amplitude for the variations of the temperature, although it must be kept in mind that it can mix different frequency for these variations. On the Northern Hemisphere scale, the Medieval Warm Epoch and the Little Ice Age clearly appears. These two periods have approximately the same amplitude in the model as in the best overlap curve as compared to 1961–1990: the period 1000–1200 is 0.26°C cooler in MILL and 0.27°C cooler in the best overlap curve. For the period 1600–1800 the cooling is of 0.52 and 0.47°C for the model and the reconstruction respectively. The correlation between the model and the best overlap curve for the mean temperature is 0.68 (statistically significant at the 99% level). This result gives confidence in our modelling of the last millennium on the Northern Hemisphere scale.

The surface temperature variations in the Southern Hemisphere are very small in the model (not shown). There are too few data collected in the Southern Hemisphere to provide robust temperature reconstructions able to provide meaningful comparison with our results at an hemispheric scale. In the Northern Hemisphere we find a strong correlation of 0.74 (statistically significant at the 99% level) between the modelled surface temperature variability in the Northern Hemisphere and the TSI variability when filtered with a cutoff value of 13 years (used to filter the Schwabe cycle). We take advantage of this strong correlation to evaluate the spatial signature of the solar forcing on surface temperature in the model through a linear regression analysis as used in Shindell et al. (2001) or Waple et al. (2002).

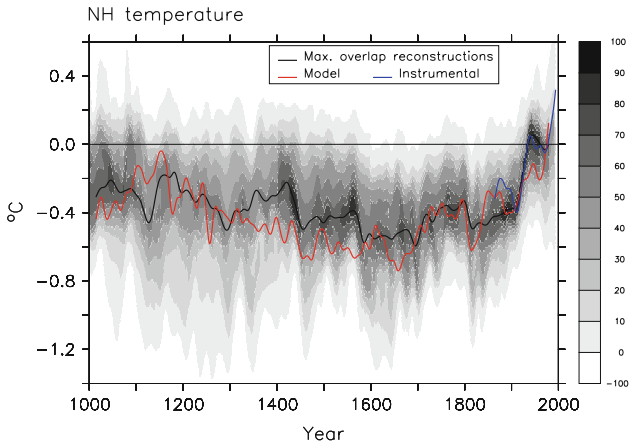

Fig. 2 Mean annual surface temperature averaged globally over the Northern Hemisphere (NH). In *red* is the MILL simulation, in *gray* are the Overlap of the published multi-decadal time scale uncertainty ranges of different temperature reconstructions identified in Table 6.1 from Jansen et al. (2007) and in *blue* is the HadCRUT3v instrumental temperature record (Brohan et al. 2006). The curve in *black* represents the maximum of the overlap probability for each time step. A low frequency filter has been applied to all curves with a cutoff of value 30 years. All temperatures represent anomalies (in °C) from the 1961 to 1990 mean

3.2 Regional temperature response to solar forcing

The fingerprint of solar forcing on the 2-m atmospheric temperature in the MILL simulation is shown in Fig. 3. The annual mean global response to changes in radiative forcing related to solar forcing is of 0.42° C/W m^{-2}. Nonetheless, it is clear from Fig. 3.a that the response is not uniform. The maximum warming occurs in the Greenland Sea where the annual mean warming reaches 3.5°C/W m^{-2}. This intense warming is associated with a negative anomaly of sea ice cover in this zone (not shown), which may amplify the solar forcing through the albedo feedback. Most of the warming occurs in the Northern Hemisphere, while the Southern Hemisphere even experiences a cooling in the Amundsen, Bellingshausen and Weddell Seas (maximum in the Amundsen Sea). This cooling signal is also related to a positive anomaly of sea ice cover (not shown). Most of the rest of the Southern Ocean does not experience any warming. The large thermal inertia of this ocean can not alone explain this signal. The increase in the zonal wind speed (and stress) between 40 and 70°S is a more plausible explanation (Fig. 3a). Indeed, the increase in the wind enhances the Deacon cell (meridional circulation of the Southern Ocean, cf. Speer et al. 2000) and the Southern Ocean mixing, which brings cold water at the surface and may explain the observed signal. Nevertheless, this cooling signal remains dependent on the model used. In particular, this model has a warm bias above the Southern Ocean in CTRL simulation due to a lack of correct ventilation of oceanic water, which may limit the validity of this result. The use of Gent and Mc Williams (1990) parametrisation may also limit a potential saturation effect from the eddies. The cooling signal could therefore be damped by these two issues, but the qualitative effect from the increase in wind over the Southern Ocean will remain.

The zonal mean response for the 2-m atmospheric temperature is represented in Fig. 3b. It shows that the response of the climate to solar forcing is asymmetric, with an increased warming from the equator to the Northern Pole, and on the other hand a decreased warming from the equator to the Southern Pole, with even a cooling from 50°S. This general response is quite reminiscent from that of global warming (see Fig. 3.9 from Trenberth et al. 2007). This pattern is similar to a meridional bipolar see-saw for the 2-m temperature, which has been hypothesized to be a pattern of climate variability during the Holocene by Denton and Broecker (2009).

4 North Atlantic Oscillation response to TSI changes

4.1 NAO and solar forcing

We now focus on the boreal winter (December–January–February) response of the climatic system to solar forcing, especially on the NAO, which has been hypothesized to be sensitive to solar forcing in the reconstructed data over Europe and North America (Shindell et al. 2001;

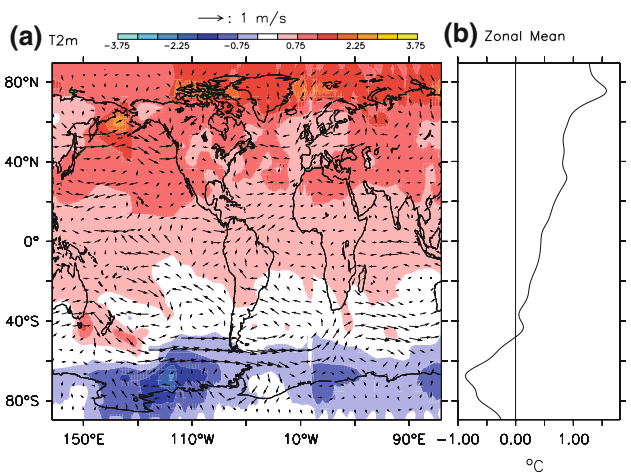

Fig. 3 **a** Regression on the solar forcing variations (Fig. 1a) of the surface atmospheric temperature at 2 m (in °C/W m^{-2}) and surface wind speed (in m s^{-1} W m^{-2}) for the period 1001–1860. All series have been low-pass filtered with a cutoff value of 13 years. Values statistically significant at the 90% level are represented by the colored shading. The contour interval is 0.5°C. **b** Zonal mean of the surface atmospheric temperature represented in **a**

Waple et al. 2002). Figure 4 shows the regression of the 2-m temperature in winter on the solar forcing, with different time lag for the former going from 0 up to 50 years. The general response at 0-year lag is similar to the annual mean one shown in Fig. 3. For a time lag of 30 years and larger (Fig. 4d–f), we notice a large warming over Northern Europe while Southern Europe does not exhibit any significant warming (contrary to its response at 0-year time lag). This signal is associated with a significantly enhanced wind speed over the Northern Europe and the Nordic Seas (Fig. 4d–f). Such a signal is reminiscent of a NAO positive phase (Hurrell 1995).

To evaluate the hypothesis of a forced NAO phase in response to solar forcing, we analyse the first Empirical Orthogonal Function (EOF) of the Sea Level Pressure (SLP) over Europe (80°W–30°E × 20°N–80°N) in boreal winter. The pattern of this first EOF is represented in Fig. 5a and compares very well with the observed one (Guemas and Salas-Mélia 2008a). It is characterized by a negative anomaly centered near Iceland and a positive anomaly centered near the Azores, leading to an anomalous enhanced wind speed over the Northern Europe, according to the geostrophic equilibrium.

The time variation of this first EOF, filtered with a 30-year cutoff value is represented in Fig. 5b for the period 1001–1860, when the anthropogenic perturbation of the climate is usually considered to be small. The reconstructed NAO index (Luterbacher et al. 2002a) for the period 1500–1860 is also represented with the same time-filtering. The simulated and reconstructed index do not compared very well for the period before 1700. On the opposite, we notice a low NAO index around 1750–1800 that appear both in the model and the reconstruction. Such a similarity could be due to chance, since the NAO is known to be chaotic (Schneider et al. 2003; Hurrell et al. 2004). To clearly validate this relationship for this period, ensemble simulation would be necessary but are out of the scope of the present study. The correlation between the low frequency of the simulated NAO and of the solar forcing for the period 1001–1860 is analysed in Fig. 5c and shows a statistically significant correlation between the two indexes of more than 0.35, with a time lag of around 40 years and more for the NAO index as compared to the solar forcing index. This significant correlation suggests a causality between the NAO index and solar forcing, and also provides an explanation for the negative NAO phase in the second part of the eighteenth century observed both in the model and reconstructions: it could be a more than 50 years delayed response to the Maunder Minimum. Volcanic eruptions during this period are very sparse and may not explain this low frequency trend.

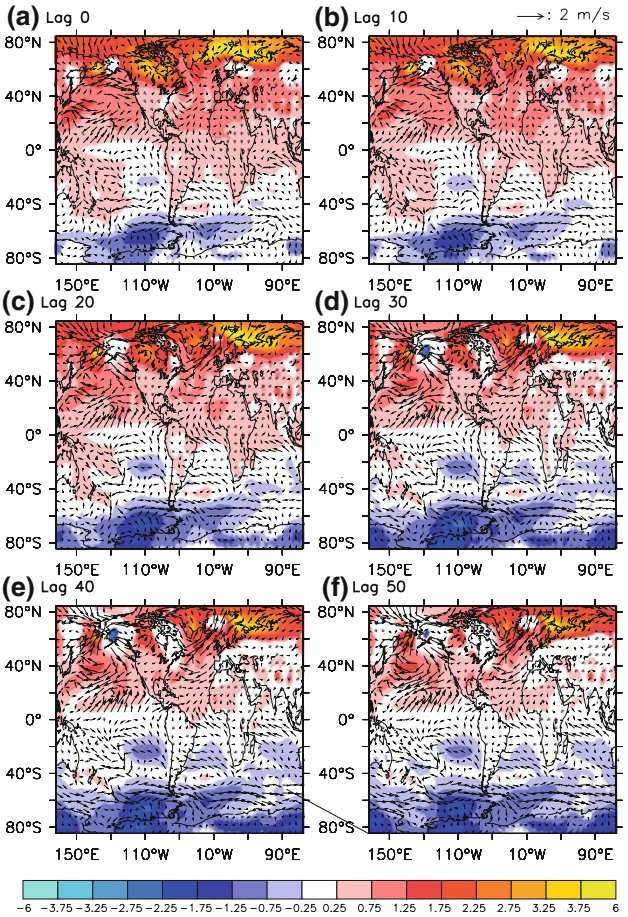

Fig. 4 In color are the regressions of mean DJF (December–January–February) temperature at 2 m on the solar index for the period 1001–1860 with different lag in the MILL simulation. The contour interval is 0.25°C / W m^{-2}. The *arrows* display the regression of the surface wind speed on the the solar index with different time lags. Only values significant at the 90% level are represented for the different variables. The panel **a** is for a 0-year lag, **b** 10-year lag, **c** 20-year lag, **d** 30-year lag, **e** 40-year lag, **f** 50-year lag of the solar forcing index

4.2 Proposed mechanism

In this section we go into the details of the possible mechanism explaining the relationship between the NAO and solar forcing. To begin with, we notice in Fig. 6 that the SLP anomalies regressed on the solar forcing concern the whole northern mid and high latitudes. The structure of the anomalies for lag larger than 20 years are reminiscent of the Arctic Oscillation pattern (AO, first EOF of the winter SLP north of 20°N, Thompson and Wallace 1998), with a negative anomaly over the North Pole and positive anomalies over the Pacific and Atlantic basins. A similar analysis as the one conducted in Fig. 5 has also been realised for the AO index. The results (not shown) are similar and even more significant than the ones obtained with the NAO index. The lag between solar variations and AO index is shorter, with a significant correlation around

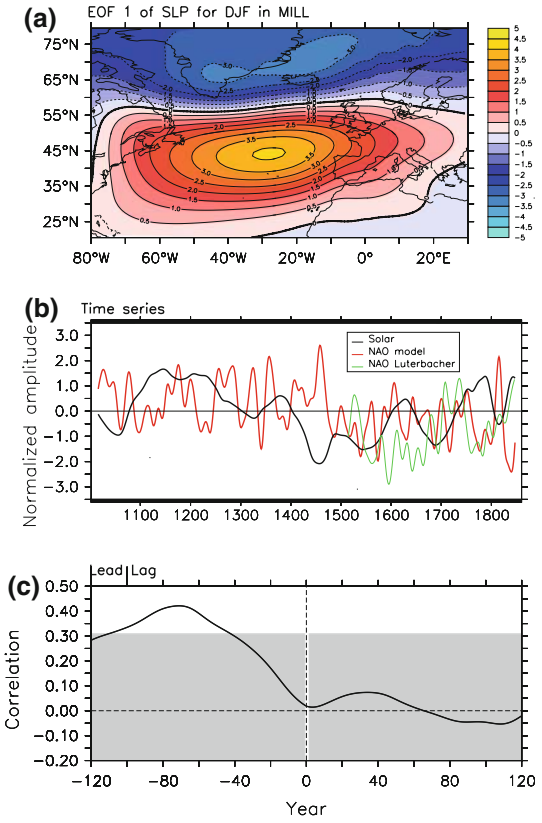

Fig. 5 **a** First EOF of the winter (DJF) Sea Level Pressure over the North Atlantic region (20°N–80°N–90°W–10°E). **b** Times series of the solar index in *black*, the principal component (PC1) of the EOF from **a** in *red* and the NAO index as reconstructed by Luterbacher et al. (2002a) in *green*. **c** Cross-correlation between the solar index and the PC1 of SLP in winter in MILL. The *grey shading* indicates 90% confidence level for zero correlation by using a bootstrap test

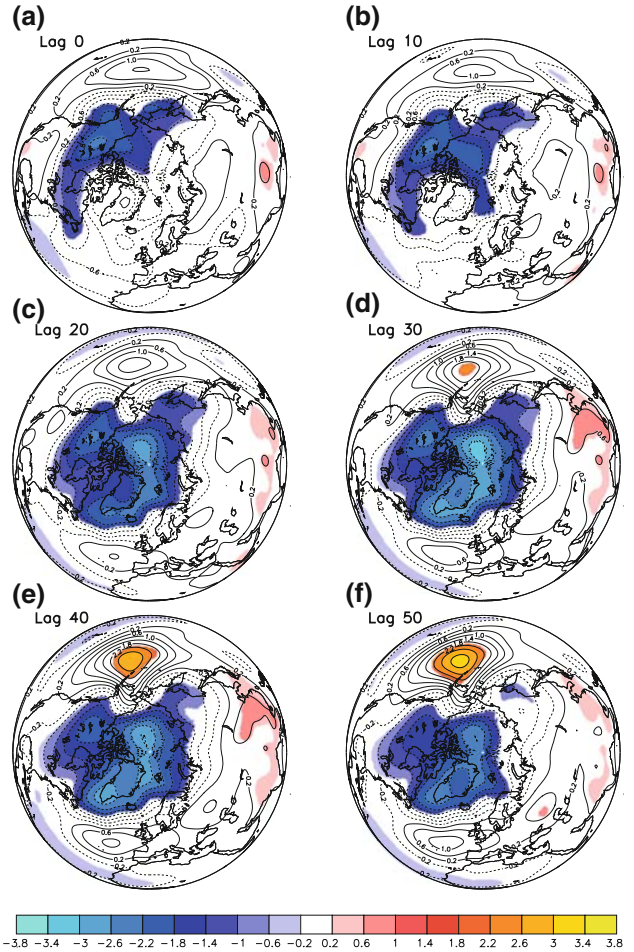

Fig. 6 In contour are the regression of the mean DJF SLP (in hPa/W m^{-2}) in MILL on the solar index for the period 1001–1860 with different time lags. Values statistically significant at the 90% level are represented by the *colored shading*. The panel **a** is for a 0-year lag, **b** 10-year lag, **c** 20-year lag, **d** 30-year lag, **e** 40-year lag, **f** 50-year lag of the solar forcing index

30-year lag, and a 0.48 maximum correlation found at 55-year lag. Indeed, we notice in Fig. 6 positive SLP anomalies over the Pacific and negative ones over the Atlantic. They are present at 0-year lag and become significant at 30- and 20-year lag respectively. Such a signature could be interprated as the excitation of a stationary wave.

This excitation is illustrated in Fig. 7, where the position of the mean jet-stream is represented by the zonal mean wind speed at 200 mb in the control simulation averaged over 1,000 years (which is similar to that in MILL). The meridional wind speed at 200 mb regressed on the solar forcing in MILL is also displayed. This type of diagnostic is useful to evaluate the excitation of quasi-barotropic atmospheric waves, which follow the wave guide formed by the jet-stream. Such a mechanism has been proposed by Branstator (2002). We see in Fig. 7 the appearance of positive and negative anomalies of meridional wind speed just north of the jet-stream maximum in the Pacific. Such a pattern is characteristic of a wave excitation that becomes mainly significant from 40-year time lag. Thus, the significant SLP anomalies that develop in the Pacific and Atlantic are associated with the excitation of a stationary wave.

The origin of this excitation can be sought in the tropical Pacific Ocean, since there exists a tropical-extratropical connection in the Pacific Ocean implying a Rossby wave radiation (Deser et al. 2004). This type of connection is actually seen in nature, notably linked with the El Nino-La Nina forcing. Meehl et al. (2008) showed the excitation of a similar SLP anomalies over the North Pacific in response to atmospheric convection anomalies in the tropical Pacific Ocean, related to the 11-year solar forcing. Moreover, a multi-models analysis led in the framework of the DYNAMITE (understanding the dynamics of the coupled climate system) project also showed that this connection is robust among a large class of OAGCMs (Cassou, personal communication). In Fig. 8, we notice an increase in

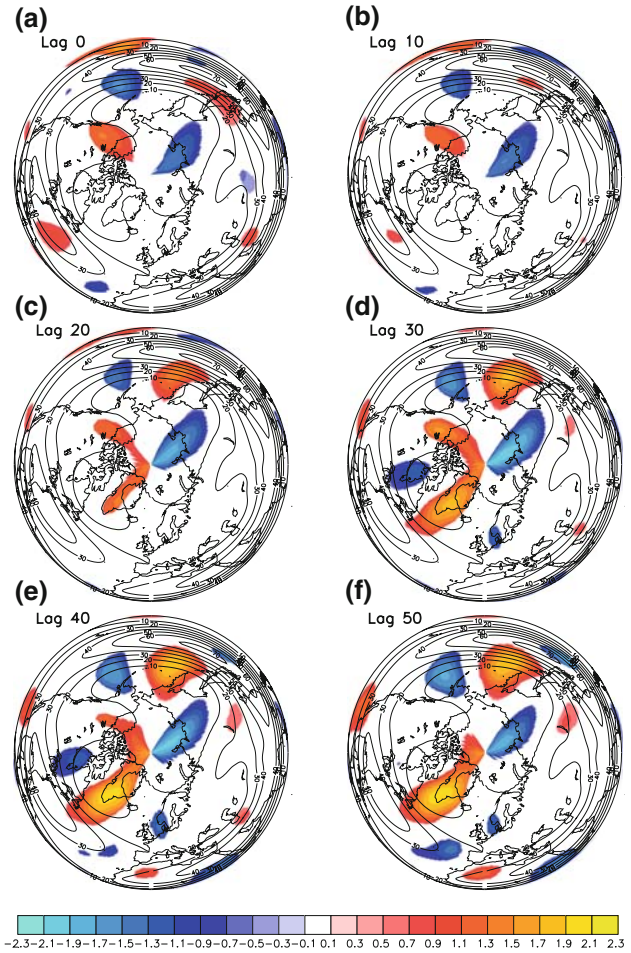

Fig. 7 In contour is the winter mean zonal wind at 200 mb in CTRL, with 10 m/s contour interval. In color are the regressions of mean DJF meridional wind at 200 mb (in m/s/W m^{-2}) in MILL on the solar index for the period 1001–1860 with different time lags. Values statistically significant at the 90% level are represented by the *colored shading*. The panel **a** is for a 0-year lag, **b** 10-year lag, **c** 20-year lag, **d** 30-year lag, **e** 40-year lag, **f** 50-year lag of the solar forcing index.

precipitation related to solar forcing centered around 10°N in the eastern part of the Pacific at 0-year lag. At 20-year lag, we notice the appearance of a pattern of precipitation decrease south of the region which experiences an increase in precipitation. This region of decrease in precipitation is enhanced for larger lag, as well as the region of increase in precipitation, which further extends towards the east. The region of increase in precipitation is related to positive SST anomalies that persist while the lag with solar forcing increases and that the solar forcing amplitude therefore decreases. Indeed, the SST anomalies elsewhere in the tropics are damped and have almost disappeared after a 30-year lag. For instance, at 40-year lag the SST anomalies are mainly significant between 5 and 20°N at the location of the positive precipitation anomalies. We therefore interpret the signal in precipitation as being due to an increase in the meridional SST gradient in the tropical Pacific, which leads to a shift of the ITCZ towards the north. The analysis of the SST difference between two Pacific boxes located between 5°N–20°N and 10°S–5°N (with a longitudinal extent going from 140 to 220°E) confirms this interpretation, since we find a significant correlation of more than 0.5 between the mean SST differences between these two boxes and the solar forcing index for a lag of 40–80 years (not shown). In the other tropical regions, there is no such large precipitation changes, which explain our focus on the Pacific basin.

The origin of the persistence of SST anomalies in the Pacific box between 5°N and 20°N (while the SST anomalies are reduced in a few decades after the TSI variations in the Pacific box between 10°S and 5°N) can be related to changes in heat flux or/and changes in heat transport. In Fig. 8, we notice an increase in the equatorial counter current in the northern hemisphere, which brings more heat from the warm pool towards the box of positive SST anomalies, and may participate to the onset of the SST anomalies (due to the fast advection of the remote anomalies by this current). The changes in the oceanic latent heat flux regressed on the solar forcing are shown in Fig. 9. We notice an increase in the latent heat released by the ocean to the atmosphere (which tends to cool the SST) at the equator in the Pacific from lag 0 to 50 years. This means that the additional incoming shortwave radiation due to the increase in solar forcing is damped by the increase in latent heat flux. This effect is similar to the process proposed by Meehl et al. (2008): a fast coupled response to solar forcing over the north equatorial Pacific, which leads to an increase in the Walker cell, decreasing cloud over the equator (Fig. 10.a) and enhancing the incoming short wave. This fast positive feedback is present in our coupled model at lag 0. It is enhanced in our model when the lag increases, because of the persistence of the SST anomalies from 5°N to 20°N. This persistence could be explained by the change in oceanic current but also by the increase in latent heat flux due to changes in wind stress (Fig 9c–f). Nevertheless, the heat flux effect in this region is almost cancelled by the decrease in shortwave radiation due to the increase in cloud over this region (Fig. 10c–f). Moreover, the large time lag found for the SST persistence rather corroborates an oceanic advective time scale. Indeed, we notice in Fig. 8 that the SST anomalies along the North Pacific subtropical gyre remains for time lags larger than 30 years. Hamon (2007) following Blanke et al. (2002) methodology used Lagrangian tracers within the same ocean GCM as used in this study to estimate the characteristic time scales of the North Pacific subpolar gyre. He found that a particle spent a mean time scale of 56 years in this gyre with a mean of 3.7 recirculations (most of the time in subsurface). Given this characteristic time scale, we argue that the transport of

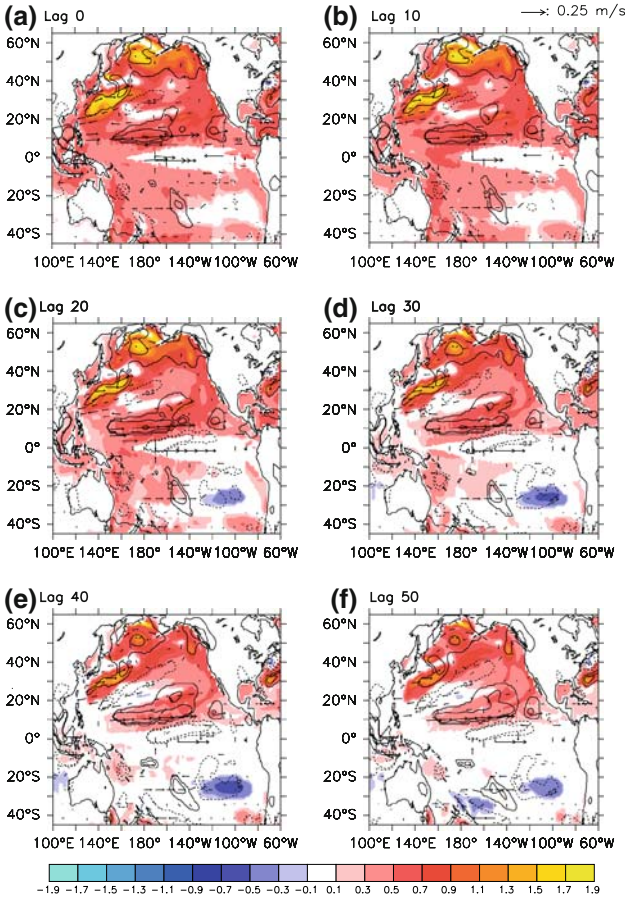

Fig. 8 In colour are the regressions on the solar index of the SST zoomed over the Pacific Ocean with a contour interval of 0.2°C/W m^{-2} for different time lags. In contour are the regressions of the precipitation on the solar index with a contour interval of 0.4 mm/day/W m^{-2}. Both regression are done for the period 1001–1860. The *arrows* display the regressions on the solar index of the oceanic surface velocity. Only values statistically significant at the 90% level are represented by the *contour*, *shading* and *arrows*. The panel **a** is for a 0-year lag, **b** 10-year lag, **c** 20-year lag, **d** 30-year lag, **e** 40-year lag, **f** 50-year lag of the solar forcing index

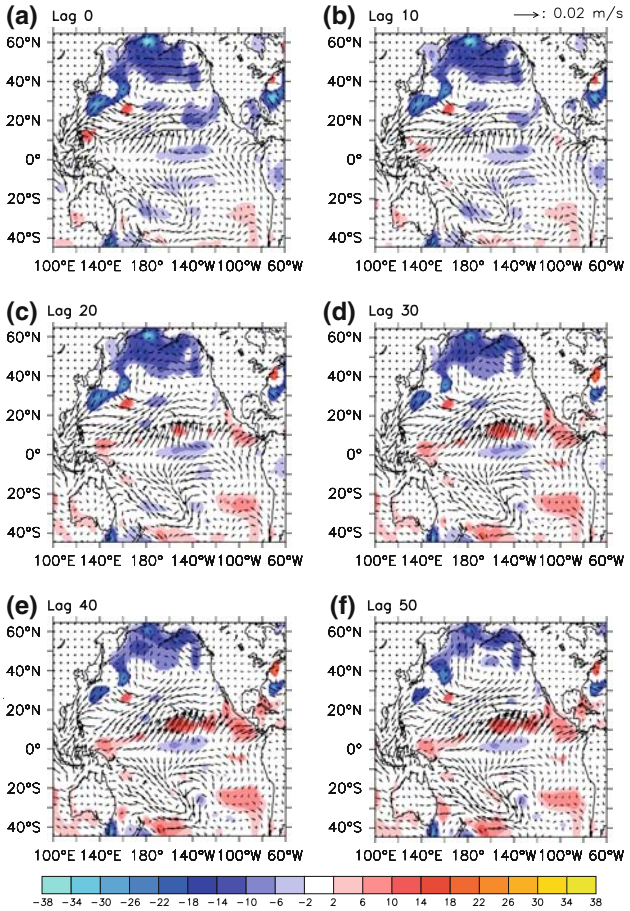

Fig. 9 Similar to Fig. 8 but with latent heat flux in color (positive when it increases the SST), and the arrows display the moisture transport in m/s/W m^{-2}

warm oceanic temperature anomalies by the subtropical gyre towards the tropical north Pacific is certainly the best candidate to explain the persistence of the SST anomalies between 5°N and 20°N in the tropical Pacific. The subduction of SST anomalies can actually avoid the damping of these anomalies by the surface fluxes and their re-emergence could explain such a large time scale. To properly confirm such a process, additional experiments will be necessary that are left to future work.

We summarize the mechanisms we propose to explain the NAO response to solar forcing in Fig. 11: an increase in TSI increases the oceanic latent heat flux in the tropics, which increases the moisture transport and the deep convection (through mass flux). This effect is enhanced by the fast feedback described in Meehl et al. (2008). The novelty of the present study is the existence of a slower process that involves the oceanic transport of temperature anomalies by the subtropical gyre towards the north west Pacific, which leads to a persistence of SST anomalies in the north tropical Pacific. This persistence increases the tropical north-south SST gradient, which shifts the ITCZ northward and enhances the atmospheric convection in the north. This in turn excites a stationary wave with a positive SLP in the Pacific and a negative SLP in the Atlantic.

5 Oceanic response in the North Atlantic to TSI changes

The impact of the NAO on the North Atlantic Ocean, and notably on the AMOC has been extensively discussed in the literature: a positive phase of the NAO is thought to enhance the convection in the Labrador Sea, and therefore the AMOC (Dickson et al. 1996; Curry et al. 1998; Eden and Willebrand 2001; Bentsen et al. 2004). The significant changes in the NAO related to the solar forcing that we observe in the MILL experiment could therefore impact on

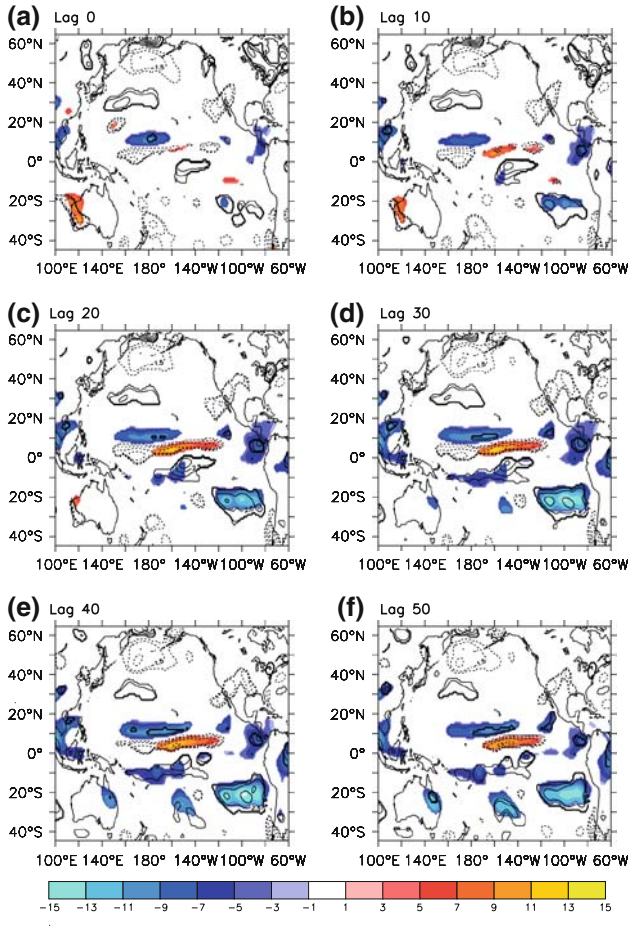

Fig. 10 Similar to Fig. 8 but with net shortwave heat flux in color (positive when it increases the SST), and the mean cloud density in contour

the AMOC. On the other hand, the increase in solar forcing could lead through radiative forcing to an SST increase in the North Atlantic that could, as for the response of the AMOC under global warming conditions (Gregory et al. 2005), weaken the AMOC. These two effects (NAO forced by TSI variations and warming due the radiative solar forcing) may oppose each other in our simulation, although their time scales are not identical since the radiative forcing effect at the top of the atmosphere is maximum for a lag around 0–10 years (not shown), while the NAO changes forced by TSI variations are significant with a 40-year lag as compared to the solar forcing index.

In Fig. 12a is shown the first EOF of the Atlantic meridional overturning streamfunction. This EOF resembles the time-mean of the AMOC (Guemas and Salas-Mélia 2008b) and therefore corresponds to a weakening-enhancement of the whole AMOC. We see in Fig. 12b, c that the principal component of this EOF is well correlated with the solar forcing index, with a maximum significant correlation of 0.54 for a lag of around 10 years as compared to the solar forcing index. The correlation corresponds to a weakening of the AMOC when the solar forcing increases. Thus, it appears that in this model, the direct effect of the radiative solar forcing dominates over the NAO forced by TSI variations for the AMOC response. Indeed, the sign of the correlation and the time scale for the lag of the response plead in favor of this interpretation.

The regression of the winter mixed layer depth (MLD) on the solar forcing index at 0-year lag is shown in Fig. 13 as well as for the surface buoyancy forcing as defined in Walin (1982). In the Labrador Sea, we notice a decrease in MLD when the solar forcing increases, which is associated to a negative buoyancy forcing related to an increase in surface heat flux (not shown). In the Nordic Seas, a positive-negative dipole of MLD anomalies represents a northward shift of the convection sites, which is related to a decrease in sea ice transport (less production in the Arctic Ocean due to increased surface temperature associated with a TSI increase) and a northward migration of the sea ice edge. Given the response of the AMOC, we suggest that the decrease in convection in the Labrador Sea explains the weakening of the AMOC after 10 years (Guemas and Salas-Mélia 2008b), while the shift of convection in the Nordic Seas has almost no effect on the deep water production.

This result does not support the assumption from Lund et al. (2006) that the AMOC was weakened during the Little Ice Age. On the opposite, we find that a solar minimum implicates an enhanced AMOC, which acts as a negative feedback on the cooling induced by the associated negative radiative forcing in the North Atlantic sector. Nevertheless, Lund et al. (2006) tried to reconstruct the Gulf Stream intensity along the Florida Straits. As they noticed, modulation of the intensity of the Gulf Stream can be due to a change in the AMOC, but also to changes in wind stress, since a large part of the subtropical gyre is wind-driven. To evaluate the changes in the barotropic gyre, we have decomposed the barotropic streamfunction in the MILL experiment using an EOF analysis. It appears that only the second EOF exhibits a significant correlation (at 50-year lag, Fig. 14b, c) with the solar forcing index. This second EOF is characterized by a dipole with a positive anomaly east of the Grand Banks and a negative one east of Florida. The Gulf Stream in the Florida Straits is not affected. The pattern of this second EOF can be explained by the anomalous wind stress over the North Atlantic regressed on the solar index with a 50-year lag, as represented in Fig. 14a. The changes in wind stress are notably related to the changes in the NAO with the solar forcing described in the previous section. Such a relationship between the NAO and a north-south displacement of the Gulf Stream has been noticed in recent observation-based data (Frankignoul et al. 2001), which gives insights on the link observed in our simulation. To conclude, we

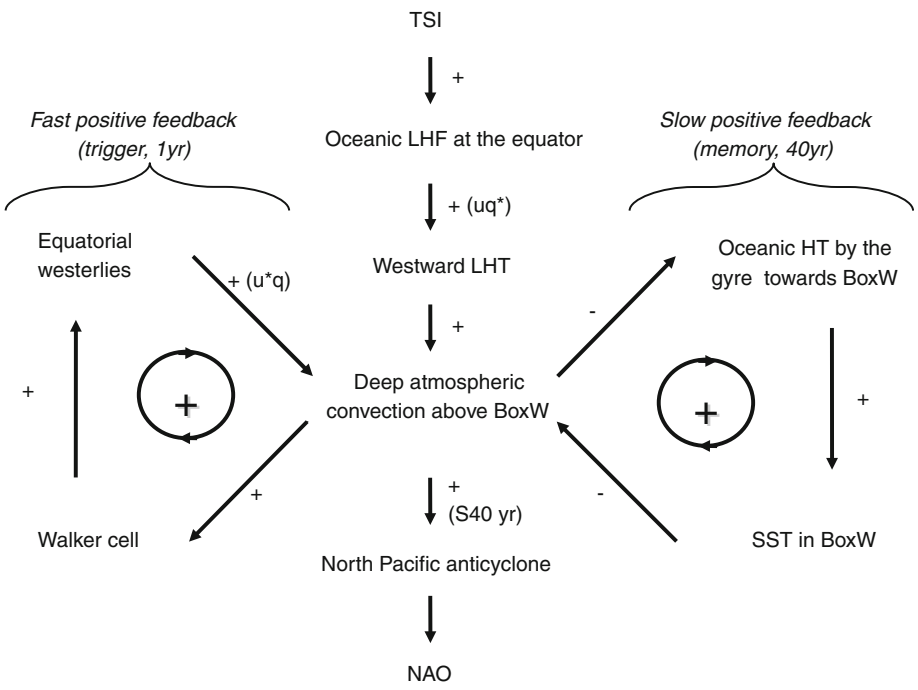

Fig. 11 Summary scheme of the mechanisms implied in the forcing of a positive NAO 40 years after a low frequency solar variations. "BoxW" is defined as the box over the Pacific ocean between 5–20°N and 140–220°E. "*u*" represents zonal wind and *q* humidity. The *stars* stands for anomalies as compared to the mean. The sign associated with each array represents the sign for the influence of the considered process. *LHF* means latent heat flux, *LHT* latent heat transport, *HT* heat transport and *S40* significant after 40 years

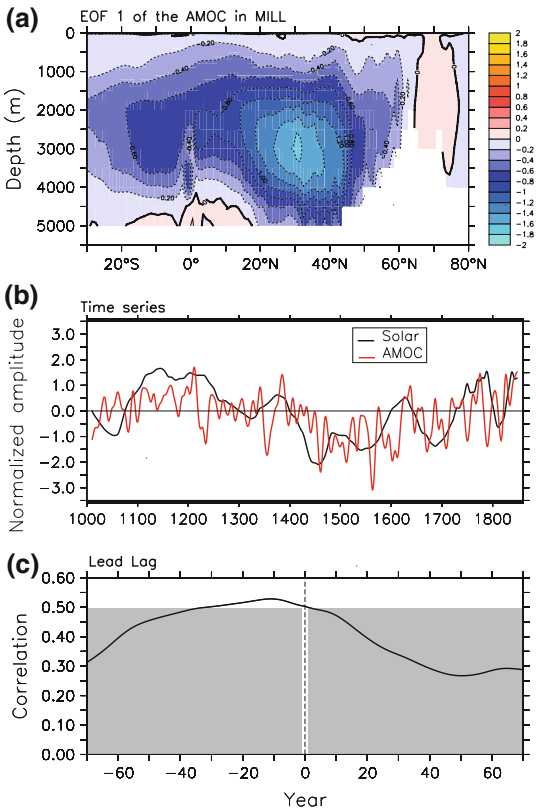

Fig. 12 **a** First EOF of the annual mean of the Atlantic meridional overturning streamfunction (in Sv) for experiment MILL. **b** Times series of the solar index in *black*, the principal component (PC1) of the EOF from **a** in *red*. **c** Cross-correlation between the solar index and the PC1 of the AMOC in MILL. The *grey shading* indicates 90% confidence level for zero correlation by using a bootstrap test

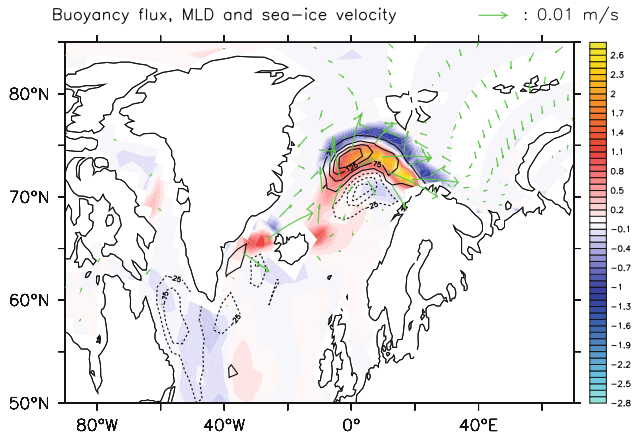

Fig. 13 Regression of the mixed layer depth in winter (*in contour*), of the annual mean buoyancy flux (*in color*) and of the annual mean sea-ice velocity (*green arrows*) over the solar forcing for the period 1001–1860.The contour interval is 50 m/W m^{-2} for the mixed layer depth and 0.01 kg/m^3/W m^{-2} for the buoyancy flux

find an enhancement of the subtropical gyre north of 35°N in response to the solar forcing, while south of 35°N, the gyre is weakened. This signal is related to changes in wind stress, while modifications in the AMOC do not affect significantly the gyre structure.

6 Discussions and conclusions

In this study, we have analysed the climate variability of the last millennium, by using a state-of-the-art OAGCM

and a few reconstructions. We have focused our attention on the low frequency response of the climate system to the low frequency solar forcing. We have shown that the model used succeeds in reproducing the low frequency temperature variability in the Northern Hemisphere. Our main result concerns the winter NAO response to the solar forcing for the period 1001–1860, which is considered to be not much perturbed by human activity. While the analysis of the temperature reconstructions over the North Atlantic sector have shown a close relationship between the increase in solar irradiance and a temperature signature that resembles a positive phase of the NAO, a lag of 10 to 30 years was found for this relationship (Waple et al. 2002). Here, we find a mechanism to explain this lag, and even larger ones. This mechanism (summarized in Fig. 11) implies the tropical Pacific response to solar forcing. The increase in TSI activates a positive feedback at 0-year lag described by Meehl et al. (2008). This positive feedback

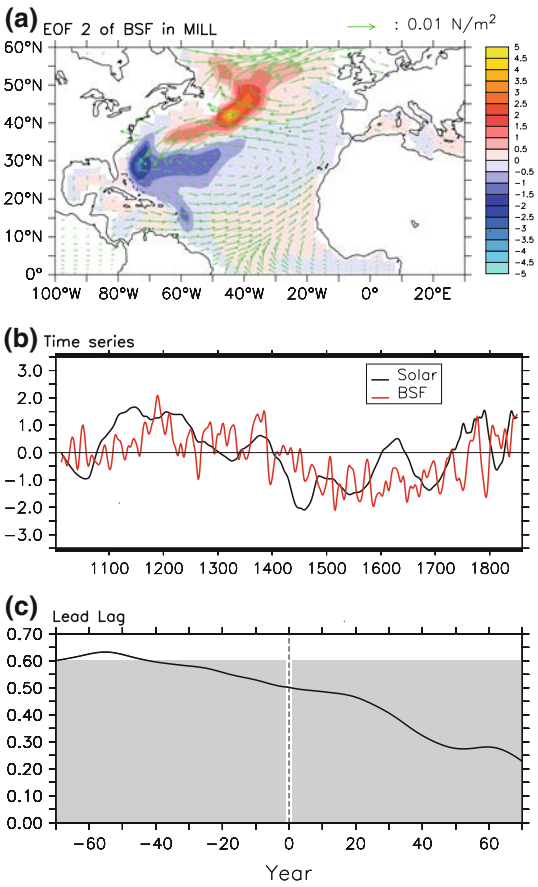

Fig. 14 **a** Second EOF of the barotropic streamfunction (BSF) over the Atlantic (0°N–60°N) for the period 1001–1860. The *green arrows* stand for regression of the annual mean wind velocity speed with a 50-year time lag on the solar forcing over the period 1001–1860. **b** Times series of the solar index in *black*, the principal component (PC2) of the EOF from **a** in *red*. **c** Cross-correlation between the solar index and the PC2 of BSF in MILL. The *grey shading* indicates 90% confidence level for zero correlation by using a bootstrap test

enhances the Walker cell over the tropical Pacific, and amplifies the atmospheric convection in the northern ITCZ. The transport of anomalous warm SST in a few decades by the North Pacific subtropical gyre makes the SST anomalies in the northeast tropical Pacific to persist for a few decades. Elsewhere in the tropical Pacific,the SST anomalies tend to disappear south of the equator 30 to 40 years after of the onset of solar variations. This leads to a tropical meridional SST gradient after 30 years, that partly shifts the ITCZ northward. This shift is associated with an enhanced atmospheric convection in the north tropical Pacific, which excites a positive SLP pressure anomaly over the North Pacific. This anomaly then propagates through the jet-stream wave guide (Branstator 2002) towards the North Atlantic, and leads to a positive NAO, significant with a 40-year time lag. This very large time lag is therefore due to a complex adjustment of the tropical Pacific Ocean, influenced by a slow coupled feedback implying the oceanic heat transport by the North Pacific subtropical gyre. This lag is also related to the very low frequency of the solar variability.

The NAO can be seen as an internal mode of variability of the atmosphere, largely chaotic (Schneider et al. 2003; Hurrell et al. 2004), and even the 1950–2000 trends in the NAO can not easily be attributed to a specific forcing (Deser and Phillips 2009). Here, in spite of the different forcing included (volcanoes, CO_2, solar), the low frequency forcing of the system by the solar forcing leads to a statistically significant low frequency forcing of the NAO, that helps to understand paleo reconstructions from Waple et al. (2002) and also from Luterbacher et al. (2002b). In particular, a delay of more than 50 years after the Maunder Minimum and a negative phase of the NAO, which appears both in the data (including instrumental after 1700 in Luterbacher et al. (2002b)) and in the model, is explained by our analysis. Nevertheless, given the chaotic nature of the NAO, an ensemble of simulations would be necessary to gain insights on this result. The variations of solar forcing in our simulation are however quite numerous and the statistical significance we find pleads in favour of our interpretation.

We have then focused our attention on the response of the North Atlantic Ocean to solar forcing. We have evaluated by using our OAGCM the hypothesis from Lund et al. (2006) of a weakening of the AMOC during the Little Ice Age, a period of low solar forcing. We find an opposite response, with a weakening of the AMOC when the solar forcing increases. We attribute this signal to a weakening of the convection in the Labrador Sea in phase with the solar forcing variations. The NAO changes forced by TSI variations do not appear to play a significant role for the forcing of the AMOC, which mostly responds to the thermal changes, as in global warming projections (Gregory

et al. 2005). Indeed, the signal of a decrease in convection in the Labrador Sea, while convection in the Nordic Seas is shifted northward but remains strong, is similar to the response observed in future climate projections using this model (Guemas and Salas-Mélia 2008b) and also other models (Wood et al. 1999; Hu et al. 2004). This result of a weakening of the AMOC with solar forcing increase is in agreement with other studies of the last millennium (Cubasch et al. 1997; Zorita et al. 2004).

Lund et al. (2006) have recorded an enhancement of the Gulf Stream rather than a direct measure of the AMOC. They admit that the variations they cornered can also be due to wind stress changes. We therefore analysed the modifications of wind stress and gyres in our experiment. We find a significant modification of the North Atlantic subtropical gyre concomitant with the wind stress modifications related to the NAO changes in response to solar forcing (e.g. with a 50-year time lag as compared to the solar forcing). These modifications however do not affect the transport across the Florida Straits, where the reconstruction from Lund et al. (2006) were made. Nevertheless, given the resolution of the ocean model (between 0.5° and 2°), this type of very thin current is not well reproduced, so that this may prevent us to observe any realistic variations of the Gulf Stream current in this region.

Finally, we would like to point out that our 2-m temperature fingerprint in response to solar forcing resembles a bipolar seesaw, with a large warming in the Northern Hemisphere (especially in high latitudes), while the Southern Hemisphere does not experience any significant warming, and even a cooling in some places in the Southern Ocean, associated with an enhancement of the zonal wind stress and an increase of mixing of the Southern Ocean. This type of response is comparable to a certain extent with the temperature response to greenhouse gases increase during the last 50 years (Trenberth et al. 2007), with a large warming at the northern high latitudes, while the Southern Ocean experiences a very small warming and even a slight increase in sea ice cover (Goosse et al. 2009). Such a bipolar seesaw is therefore not related to the changes in the AMOC, which in our model goes in the opposite way with the solar forcing, and rather feeds back negatively on this signal. Thus, any bipolar seesaw-like signals in the archive of the past (Denton and Broecker 2009), do not necessarily corroborate AMOC changes, but could be only related to the thermal response of the climate, influenced by its different distribution of continents and oceans between the two hemispheres.

To conclude, we argue that additional data for the beginning of the last millennium would be very useful to validate the existence of the mechanisms we propose. In particular oceanic data for the whole millennium is clearly missing as compared to the quantity of land reconstructions. Recent efforts for obtaining oceanic core data with a high temporal resolution (Lund et al. 2006; Sicre et al. 2008) should be encouraged. This will help to improve our understanding of the low frequency of the ocean and the mechanisms explaining the low frequency of the natural climate variability. The analysis of the high frequency related to volcanic eruptions will be analysed in a companion paper notably by using this simulation and a new reconstruction of climate variability over Europe (Guiot et al. 2010).

Acknowledgments We thank Hugues Goosse, Joel Guiot and Christoph Raible for very constructive discussion about the results presented here. We thank Tim Osborn for his help concerning the overlap reconstructed temperature. This paper is a contribution to the project ESCARSEL funded by the French Agency for National Research (ANR VMC 2006). The use of statpack, safo and ferret softwares is acknowledged. The help of Patrick Brockmann and Eric Maisonnave has improved the quality of the figures.

References

Ammann CM, Joos F, Schimel DS, Otto-Bliesner BL, Tomas RA (2007) Solar influence on climate during the past millennium: results from transient simulations with the NCAR Climate System Model. Proc Natl Acad Sci 104:3713–3718

Bard E, Raisbeck G, Yiou F, Jouzel J (2000) Solar irradiance during the last 1200 years based on cosmogenic nuclides. Tellus B 52:985–992

Bentsen M, Drange H, Furevik T, Zhou T (2004) Simulated variability of the Atlantic meridional overturning circulation. Clim Dyn 22:701–720

Berger A (1978) Long-term variation of caloric solar radiation resulting monthly and latitudinally varying volcanic forcing dataset in simulations from the earthGs orbital elements. Quat Res 9:139G167

Bertrand C, Loutre M, Crucifix M, Berger A (2002) Climate of the last millennium: a sensitivity study. Tellus 54A:221–244

Blanke B, Arhan M, Speich S, Pailler K (2002) Diagnosing and picturing the north atlantic segment of the global conveyor belt by means of an ocean general circulation model. J Phys Oceanogr 32:1430–1451

Blanke B, Delecluse P (1993) Variability of the tropical Atlantic ocean simulated by a general circulation model with two different mixed layer physics. J Phys Oceanogr 23:1363–1388

Bradley RS, Jones PD (1993) "Little Ice Age" summer temperature variations: their nature and relevance to recent global warming trends. Holocene 3:367–376

Branstator G (2002) Circumglobal teleconnections, the jetstream waveguide, and the North Atlantic Oscillation. J Clim 15:1983–1910

Brohan P, Kennedy JJ, Harris I, Tett S, Jones P (2006) Uncertainty estimates in regional and global observed temperature changes: a new dataset from 1850. J Geophys Res 111:D12106

Cassou C, Terray L (2001) Dual influence of Atlantic and Pacific SST anomalies on the North Atlantic/Europe Winter Climate. Geophys Res Lett 28:3195–3198

Chapelon N, Douville H, Kosuth P, Oki T (2002) Off-line simulation of the Amazon water balance: a sensitivity study with implications for GSWP. Clim Dyn 19:141–154

Crowley TJ (2000) Causes of climate change over the past 1000 years. Science 289:270–277
Cubasch U, Voss R, Hegerl GC, Waszkewitz J, Crowley TJ (1997) Simulation of the influence of solar radiation variations on the global climate with an ocean–atmosphere general circulation model. Clim Dyn 33:757–767
Curry RG, McCartney MS, Joyce TM (1998) Oceanic transport of subpolar climate signals to mid-depth subtropical waters. Nature 391:575–577
Denton GH, Broecker WS (2009) Wobbly ocean conveyor circulation during the Holocene? Quat Sci Rev 27:1939–1950
Déqué M et al (1999) ARPEGE version 3, documentation algorithmique et mode dGemploi. Tech. rep., available from CNRM/GMGEC, Météo-France, 42 avenue G. Coriolis, 31057 Toulouse, France (in French)
Deser C, Phillips A (2009) Atmospheric circulation trends, 1950–2000: the relative roles of sea surface temperature forcing and direct atmospheric radiative forcing. J Clim 22:396–413
Deser C, Phillips AS, Hurrell JW (2004) Pacific interdecadal climate variability: linkages between the Tropics and North Pacific during boreal winter since 1900. J Clim 17:3109–3124
Dickson RR, Lazier JJ, Meincke J, Rhines P, Swift J, (1996) Longterm coordinated changes in the convective activity of the North Atlantic. Prog Oceanogr 38:241–295
Douville H, Royer J-F, Mahfouf J-F (1995) A new snow parametrization for the Météo-France climate model. Part I: validation in stand-alone experiments. J Clim 12:21–35
Duchon CE (1979) Lanczos filtering in one and two dimensions. J Appl Meteorol 18:1016–1022
Ebisuzaki W (1997) A method to estimate the statistical significance of a correlation when the data are serially correlated. J Clim 10:2147–2153
Eddy J (1976) The Maunder minimum. Science 192:1189–G1202
Eden C, Willebrand J (2001) Mechanism of interannual to decadal variability of the north atlantic circulation. J Clim 14:2266–2280
Forster P et al (2007) Changes in Atmospheric Constituents and in Radiative Forcing. In: Climate Change 2007: The Physical Science Basis. Contribution of Working Group I to the Fourth Assessment Report of the Intergovernmental Panel on Climate Change. Cambridge University Press, Cambridge, United Kingdom and New York, NY, USA, pp 129–234
Foukal P, North G, Wigley T (2004) A stellar view on solar variations and climate. Science 306:68G69
Frankignoul C, de Coetlogon G, Joyce T, Dong S (2001) Gulf Stream variability and ocean–atmosphere interactions. J Phys Oceanogr 31:3516–3529
Gent PR, Mc Williams JC (1990) Isopycnal mixing in ocean circulation models. J Phys Oceanogr 20:150–155
Gibelin AL, Déqué M (2003) Anthropogenic climate change over the Mediterranean region simulated by a global variable resolution model. Clim Dyn 20:327G–339
Goosse H, Lefebvre W, de Montety A, Crespin E, Orsi A (2009) Consistent past half-century trends in the atmosphere, the sea ice and the ocean at high southern latitudes. Clim Dyn. doi:doi10.1007/s00382-008-0500-9
Gregory J et al (2005) A model intercomparison of changes in the Atlantic thermohaline circulation in response to increasing atmospheric CO_2 concentration. Geophys Res Let 32
Grieser J, Schönwiese CD (1999) Parameterization of spatio-temporal patterns of volcanic aerosol induced stratospheric optical depth and its climate radiative forcing. Atmosfera 12:111–133
Guemas V, Salas-Mélia D (2008a) Simulation of the Atlantic meridional overturning circulation in an atmosphere–ocean global coupled model. Part I : a mechanism governing the variability of ocean convection in a preindustrial experiment. Clim Dyn 31:29–48
Guemas V, Salas-Mélia D (2008b) Simulation of the Atlantic meridional overturning circulation in an atmosphere–ocean global coupled model. Part II : a weakening in a climate change experiment—a feedback mechanism. Clim Dyn 30:831–844
Guiot J, Corona C, ESCARSEL members (2010) Growing season temperature in europe and climate forcings for the last 1400 years. PLoS ONE (submitted)
Hamon M (2007) La circulation de l'océan global décrite par une trajectoire lagrangienne. M.S. thesis, Université de Bretagne Occidentale (in French)
Hegerl G et al (2007) Understanding and attributing climate change. In: Climate change 2007: the physical science basis. Contribution of Working Group I to the Fourth Assessment Report of the Intergovernmental Panel on Climate change. Cambridge University Press, Cambridge, UK and New York, NY, USA, pp 663–746
Hu AX, Meehl GA, Washington WM, Dai AG (2004) Response of the Atlantic thermohaline circulation to increased atmospheric CO_2 in a coupled model. J Clim 17:4267–4279
Hunke EC, Dukowicz JK (1997) An elasticGviscousGplastic model for sea ice dynamics. J Phys Oceanogr 27:1849G–1867
Hunke EC, Lipscomb WH (2002) CICE: the Los Alamos sea ice model, documentation and software UserGs Manual. T-3 Fluid Dynamics Group. Tech rep lacc-98G16 v.3, Los Alamos National Laboratory
Hurrell JW (1995) Decadal trends in the North Atlantic Oscillation: regional temperatures and precipitation. Science 269:676–679
Hurrell JW, Hoerling MP, S PA, Caron J, Yin J (2004) Twentieth century North Atlantic climate change. Part I: assessing determinism. J Atmos Sci 60:1504–1521
Huybers P, Curry W (2006) Links between annual, milankovitch and continuum temperature variability. Nature 441:329–332
Jansen E et al (2007) Palaeoclimate. In: Climate change 2007: the physical science basis. Contribution of Working Group I to the Fourth Assessment Report of the Intergovernmental Panel on Climate change. Cambridge University Press, Cambridge, UK and New York, NY, USA, pp 433–498
Jones P, Osborn T, Briffa K (2001) The evolution of climate over the last millennium. Science 292:662–G667
Keenlyside NS, Latif M, Jungclaus J, Kornblueh L, Roeckner E (2008) Advancing decadal-scale climate prediction in the North Atlantic sector. Nature 453:84–88. doi:10.1038/nature06921
Lamb H (1965) The early medieval warm epoch and its sequel. Palaeogeogr Palaeoclimatol Palaeoecol 1:13–37
Lean J, Beer J, Bradley R (1995) Reconstruction of solar irradiance since 1610: implications for climate change. Geophys Res Lett 22:3195–G3198
Lean J, Wang Y, Sheeley N (2002) The effect of increasing solar activity on the sunGs total and open magnetic flux during multiple cycles: Implications for solar forcing of climate. Geophys Res Lett. doi:10.1029/2002GL015880
Levitus S (1982) Climatological atlas of the world ocean. Professional paper, NOAA/GFDL
Lund DC, Lynch-Stieglitz J, Curry WB (2006) Gulf Stream density structure and transport during the past millennium. Nature 444:601–604
Luterbacher J, Xoplaki E, Rickli R, Gyalistras D, Schmutz C, Wanner H (2002b) Reconstruction of sea level pressure fields over the Eastern North Atlantic and Europe back to 1500. Clim Dyn 18:545–561
Luterbacher J et al (2002a) Extending north atlantic oscillation reconstructions back to 1500. Atmos Sci Lett. doi:10.1006/asle.2001.0044
Madec G, Chartier M, Delecluse P, Crépon M (1991) A three-dimensional numerical study of deep water formation in the Northwestern Mediterranean Sea. J Phys Oceanogr 21:1349G–1371

Madec G, Delecluse P, Imbard M, L+vy C (1998) OPA version 8. Ocean general circulation model reference manual. Rapp. Int., LODYC, France, p 200

Mahfouf JF, Manzi A, Noilhan J, Giordani H, Déqué M (1995) The land surface scheme ISBA within the Météo-France climate model ARPEGE. Part I. Implementation and preliminary results. J Clim 8:2039–2057

Mann M, Bradley R, Hughes M (1998) Global-scale temperature patterns and climate forcing over the past six centuries. Nature 392:779–787

Mann ME, Zhang ZH, Hughes MK, Bradley RS, Miller SK, Rutherford S, Fenbiao N (2008) Proxy-based reconstructions of hemispheric and global surface temperature variations over the past two millennia. Proc Natl Acad Sci 105:13252–13257

Masson V, Champeaux J-L, Chauvin F, Meriguet C, Lacaze R (2003) A global database of land surface parameters at 1-km resolution in meteorological and climate models. J Clim 16:1261–1282

Meehl G, Arblaster J, Branstator G, van Loon H (2008) A coupled air–sea response mechanism to solar forcing in the Pacific region. J Clim 21:2883–2897

Moberg A, Sonechkin DM, Holmgren K, Datsenko NM, Karlen W (2005) Highly variable northern hemisphere temperatures reconstructed from low- and high-resolution proxy data. Nature 433:613–617

Muscheler R, Joos F, Beer J, Muller SA, Vonmoosc M, Snowballd I (2007) Solar activity during the last 1000 yr inferred from radionuclide records. Quat Sci Rev 26:82–97

Oki T, Sud YC (1998) Design of total runoff integrating pathways (TRIP). A global river channel network. Earth Interact 2:1–37

Ottera OH (2008) Simulating the effects of the 1991 Mount Pinatubo volcanic eruption using the ARPEGE atmosphere general circulation model. Adv Atmos Sci 25:213–226

Paillard D (2008) From atmosphere, to climate, to Earth system science. Interdiscip Sci Rev 33:25–35

Paulson CA, Simpson JJ (1977) Irradiance measurements in the upper ocean. J Phys Oceanogr 7:952G–956

Ramankutty N, Foley J (1999) Estimating historical changes in global land cover: croplands from 1700 to 1992. Global Biogeochem Cycles 13:997–1027

Salas-Mélia D (2002) A global coupled sea ice-ocean model. Ocean Model 4:137–172

Salas-Mélia D et al (2005) Description and validation of the CNRM-CM3 global coupled model. Tech rep, CNRM technical report 103. URL http://www.cnrm.meteo.fr/scenario2004/paper_cm3.pdf, available from CNRM/GMGEC, 42 ave. G.Coriolis, 31057 Toulouse, France

Schneider B, Latif M, Schmittner A (2007) Evaluation of different methods to assess model projections of the future evolution of the atlantic meridional overturning circulation. J Clim 20:2121–2132

Schneider EK, Bengtsson L, Hu Z (2003) Forcing of northern hemisphere climate trends. J Atmos Sci 60:1504–1521

Shindell D, Schmidt G, Miller R, Mann M (2003) Volcanic and solar forcing of climate change during the preindustrial era. J Clim 16:4094–4107

Shindell DT, Schmidt GA, Mann ME, Rind D, Waple A (2001) Solar forcing of regional climate change during the Maunder minimum. Science 294:2149–2152

Sicre MA et al (2008) Decadal variability of sea surface temperatures off North Iceland over the last 2000 yrs. Earth Planet Sci Lett. doi:10.1016/j.epsl.2008.1001.101

Speer K, Rintoul SR, Sloyan B (2000) The diabatic Deacon cell. J Phys Oceanogr 12:3212–3222

Stendel M, Mogensen IA, Christensen JH (2006) Influence of various forcings on global climate in historical times using a coupled atmosphere–ocean general circulation model. Clim Dyn 26:1–15

Thompson DWJ, Wallace JM (1998) The Arctic Oscillation signature in the wintertime geopotential height and temperature fields. Geophys Res Lett 25:1297–1300

Thorndike AS, Rothrock DA, Maykut GA, R C (1975) The thickness distribution of sea ice. J Geophys Res 80:4501–4513

Trenberth K et al (2007) Observations: surface and atmospheric climate change. In: Climate change 2007: the physical science basis. Contribution of Working Group I to the Fourth Assessment Report of the Intergovernmental Panel on Climate change. Cambridge University Press, Cambridge, UK and New York, NY, USA, pp 235–336

Valcke S, Declat D, Redler R, Ritzdorf H, Schoenemeyer T, Vogelsang R (2004) In: Proceedings of the 6th International Meeting, High performance computing for computational science, Vol. 1. Universidad Politecnica de Valencia, Valencia, Spain., the PRISM Coupling and I/O System. VECPAR'04

Walin G (1982) On the relation between sea-surface heat flow and thermal circulation in the ocean. Tellus 34:187–195

Waple AM, Mann ME, Bradley RS (2002) Long-term patterns of solar irradiance forcing in model experiments and proxy based surface temperature reconstructions. Clim Dyn 18:563–578

Wood RA, Keen AB, Mitchell JFB, Gregory JM (1999) Changing spatial structure of the thermohaline circulation in response to atmospheric CO_2 forcing in a climate model. Nature 399:572–575

Zorita E, von Storch H, Gonzalez-Rouco FJ, Cubasch U, Luterbacher JU, Legutke S, Fischer-Bruns I, Schlese U (2004) Climate evolution in the last five centuries simulated by an atmosphere–ocean model: global temperatures, the North Atlantic Oscillation and the Late Maunder minimum. Meteorologische Zeitschrift 13:271–289